El Niño influence on potential maize yield in Iberian Peninsula

Mirian Capa-Morocho, Belén Rodríguez-Fonseca and Margarita Ruiz-Ramos

ABSTRACT: El Niño phenomenon is the leading mode of sea surface temperature interannual variability. It can affect weather patterns worldwide and therefore crop production. Crop models are useful tools for impact and predictability applications, allowing to obtain long time series of potential and attainable crop yield, unlike to available time series of observed crop yield for many countries. Using this tool, crop yield variability in a location of Iberia Peninsula (IP) has been previously studied, finding predictability from Pacific El Niño conditions. Nevertheless, the work has not been done for an extended area. The present work carries out an analysis of maize yield variability in IP for the whole 20th century, using a calibrated crop model at five contrasting Spanish locations and reanalyses climate datasets to obtain long time series of potential yield. The study tests the use of reanalysis data for obtaining only climate-dependent time series of crop yield for the whole region, and to use these yield to analyse the influences of oceanic and atmospheric patterns. The results show a good reliability of reanalysis data. The spatial distribution of the leading principal component of yield variability shows a similar behaviour over all the studied locations in the IP. The strong linear correlation between El Niño index and yield is remarkable, being this relation non-stationary on time, although the air temperature–yield relationship remains on time, being the highest influences during grain filling period. Regarding atmospheric patterns, the summer Scandinavian pattern has significant influence on yield in IP. The potential usefulness of this study is to apply the relationships found to improving crop forecasting in IP.

KEY WORDS maize yield; El Niño; La Niña; crop simulation; Iberian Peninsula; SST; reanalysis dataset

1. Introduction

Variability of agricultural production has a major impact on farm economies, agricultural markets, and food security (Godfray *et al.*, 2010). Climate variability and changes on frequency of extreme events have a direct influence on the quantity and quality of agricultural production, in many cases, with adverse effects (Salinger *et al.*, 2005). Therefore, a comprehensive consideration of the potential impacts of climate on agriculture is necessary (Rosenzweig and Liverman, 1992). Climate science may also benefit from such assessment. Potential crop yield can provide new qualitative information regarding climate variability by integrating the effects of weather factors during the crop cycle (Saue and Kadaja, 2009; Capa-Morocho *et al.*, 2014). This potential yield is defined as the yield of a cultivar when grown in environments to which it is adapted, with unlimited supplied of nutrients and water, and stressful factors such as pests, diseases, weeds, lodging, and other stresses effectively controlled (Evans and Fischer, 1999). In contrast, former research on the subject used the historical or observed crop yield that includes the influence of other factors such as soil variability, management efficiency, biotic and abiotic stresses, technology trends, and even agricultural policies and market pressures (Lobell *et al.*, 2009).

Assessment of climate risk causing production losses has been accomplished by crop modelling (Meinke and Hammer, 1995; Hammer *et al.*, 2000; Potgieter *et al.*, 2005). Crop models have been important tools for impact and predictability applications (Shin *et al.*, 2010). They allow for obtaining long time series of potential and attainable crop yield for many countries unlike to available time series of (1) observed, historical crop yields, and (2) simulated yields with observed weather data, whose length is constraint by the availability of the historical meteorological records. Further extension of the potential yield time series could be important to study the stationary and multidecadal modulation of crop yield by teleconnection patterns such as El Niño (Capa-Morocho *et al.*, 2014). This kind of relationships could benefit crop forecasting, and improving such prediction is currently needed to establish early warning systems and design crop management adaptations that take advantage of favourable conditions or reduce the effects of adverse conditions in present and future climate.

Climate variables are determinant factors for yield formation and therefore are essential inputs for crop simulation models. Consequently, a comprehensive evaluation

of crop potential yield simulated with various climate data sources is necessary to improve the current practice of crop yield forecasting and projection (Shin *et al.*, 2010), whenever the reliability of available climate datasets is evaluated. For such improvement, the crop models calibrated in a specific site for local varieties, fed with long-term reanalysis climate datasets, are powerful tools for generating only climate-dependent time series of historical potential yield at regional level.

In a former study, the variability of potential yield of summer crops in the Northwest (NW) of Iberian Peninsula (IP) was studied using auxiliary reanalysis data (Capa-Morocho *et al.*, 2014). Apart from the reliability study, the results showed the influence of the sea surface temperature (SST) on the local crop yield variability, detecting a relation between crop development and growth and El Niño phenomenon with 1 year in advance. Moreover, the statistical relation between simulated potential yield and anomalous SSTs in the Equatorial Pacific was stronger than that between the NW-IP atmospheric climate data and SST, i.e. between the climate variables used to run the crop model and SST.

These results could be a major finding to improve crop predictability if they could be extended to the whole IP and other European regions. For this reason, in the present work, the analysis is extended to the whole IP by running the crop model at five contrasting locations spread across main Spanish agricultural areas. The aims of this study are to confirm the El Niño–yield relationship in IP, and to further investigate the spatial configuration of the teleconnection. For that purpose, several steps are needed (1) to assess the reliability of reanalysis datasets for obtaining long series potential crop yield in IP, (2) to define the leading mode of potential yield variability using the five selected locations to determine the regions in the IP with a similar behaviour, (3) to compare it with the spatial configuration in crop yields associated with El Niño, and (4) to analyse the variability pattern of atmospheric climate variables to infer hypothesis about the eco-physiological mechanism behind crop response.

The paper structure is as follows: in Section 2, the data and methods used in this study are described; Section 3 provides the results including crop simulations with observed data *versus* reanalysis data; the leading mode of spatial distribution of yield variability and temperature variability in IP; relationships between yield, temperature and El Niño index, and the spatial configuration of the teleconnection. Some specific aspects are discussed. In Section 4, a general discussion is given, followed by concluding remarks in Section 5.

2. Data and methods

2.1. Study sites

Five sites (Figure 1) have been selected for study, covering the main agricultural areas of Spain: Lugo in NW, Lérida in Northeast (NE), Madrid in Central Spain, Albacete in Southeast (SE), and Córdoba in South (S). These

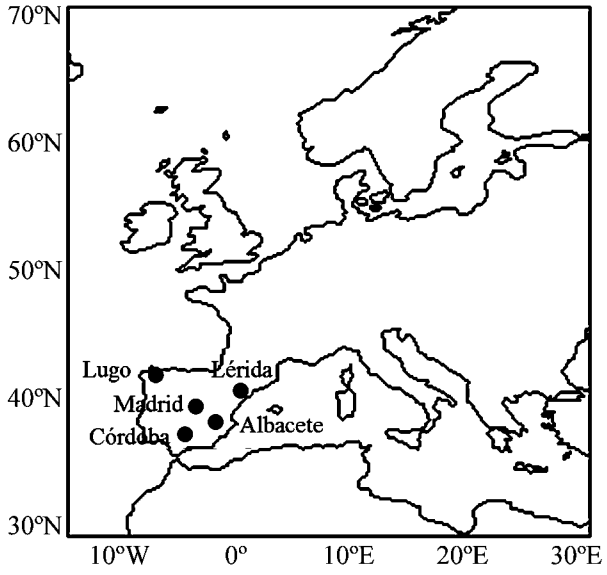

Figure 1. The study area. Locations in the IP where the crop model is calibrated and validated and crop simulations are conducted.

sites are representative agricultural locations with contrasting altitudes, temperature, and precipitation regimes (Table 1), and they are selected because crop data from field experiments and weather station data are available to calibrate the crop model and evaluate reanalysis data (see references in Table 1).

2.2. Crop modelling

Simulated yields are computed with CERES-maize model (Jones and Kiniry, 1986), which is included in Decision Support System for Agrotechnology Transfer (DSSAT v.4.5. Hoogenboom *et al.*, 2010). CERES-maize is a dynamic eco-physiological model that integrates the effects of crop genotype, soil profile, weather data, and management options. The crop model requires daily data of maximum and minimum surface temperature (T_{max} and T_{min}), precipitation (Prec), and incoming solar radiation (Rad). It computes plant growth and development processes on a daily basis in a specific location from sowing to crop maturity. The crop model uses mean temperature (T_{mean}) to compute the thermal time (sum of temperatures above a base temperature that makes crop development to progress). As a result, the impact of weather, soils, and management decisions on crop yield can be estimated (Phillips *et al.*, 1998; Shin *et al.*, 2010).

Irrigated maize is chosen as a reference for representing summer crops because it is one of the main summer field crops in IP. Sowing date is usually April (end of March in the most Southern location, Córdoba) (Table 1) and harvest date is generally from August to September. Crop varieties, management, and soil profiles are set for each location to represent current common cultivar, practices, and soils, respectively, as are specified in Table 1. Field data for CERES-maize model calibration and validation were collected using crop data from previous experimental sites at the plot scale (Maturano, 2002; López-Cedrón *et al.*, 2005; Lizaso *et al.*, 2010; Gabriel and Quemada, 2011;

Table 1. Main features of studied locations and field data (crop varieties, management, soil type) retrieved for CERES-maize model calibration and validation.

Location	Lugo	Lérida	Madrid	Albacete	Córdoba
Longitude	7.45°W	0.60°E	3.72°W	1.85°W	4.78°W
Latitude	43.10°N	41.63°N	40.30°N	38.95°N	37.88°N
Altitude (m)	452	190	617	704	90
T_{max} (°C)[a]	17.52	21.44	20.87	20.80	25.13
T_{min} (°C)[a]	6.36	8.74	9.30	7.94	11.4
T_{mean} (°C)[a]	11.94	15.09	15.08	14.37	18.27
Annual precipitation (mm)[a]	1103	351	372	366	624
Climate classification (Kottek *et al.*, 2006)	Warm temperate, summer dry, warm summer (Csb)	Warm temperate, fully humid, hot summer (Cfa)	Warm temperate, summer dry, hot summer (Csa)	Arid, summer dry, cold arid (Bsk)	Warm temperate, summer dry, hot summer (Csa)
Crop modelling					
Variety	Clarica (FAO 300)	Eleonora (FAO 700)	G-98 Pioneer (FAO 700)	Prisma (FAO 700)	Helen (FAO 700)
Sowing date	20 April	01 April	10 April	15 April	21 March
Soil	Typic Haplumbrept	Petrocalcic Calcixerept	Typic Calcixerept	Calcixerollic-Xerochrepts	Xerofluvent
Calibration and validation field data					
Years	1998, 1999, 2000, 2001, 2002, 2003	2003, 2004, 2005	2007, 2008, 2009, 2010	1999, 2003	2005, 2006, 2007, 2008, 2009, 2010
Number of data	8	9	6	7	16
References	López-Cedrón *et al.* (2005)	Lizaso *et al.* (2010)	Gabriel and Quemada (2011)	Maturano (2002)	Gabaldon-Leal *et al.* (2015)

References of field experiments are included. [a]Baseline: 1986–2010.

Gabaldon-Leal *et al.*, 2015). The experiments included between 2 and 6 years of data on maize phenology (sowing, anthesis or flowering, and maturity dates), yield, and biomass for several treatments of nitrogen fertilization levels and/or different sowing dates per year, depending on the experiment (number of treatments for each location is in Table 1). Genetic coefficients were calibrated first to match correctly crop phenology and later to approximate measured grain yield and crop biomass.

Once calibrated and validated, the simulation experiment is set to obtain potential yields: yield under non-limiting water and nitrogen conditions. Thus, the simulated processes are affected by the main environmental variables: daily solar radiation and maximum and minimum temperature. Therefore, it is important to stress that precipitation does not influence yield in these simulations. The crop model only uses precipitation to calculate the amount of irrigation water required by crop. Thus, the analysis considered only temperature and radiation effects on potential yield.

2.3. Weather and climate data

Crop simulations are conducted with both observed and reanalysis climate datasets. Observed climate data corresponds to weather stations from the State Meteorological Agency of Spain (AEMET), selecting the closest station to each location that in turn spans different periods (Table 2). Reanalysis climate data are obtained from various sources:

- National Oceanic Atmospheric Administration (NOAA): Twentieth Century Reanalysis Project (Compo *et al.*, 2011) from 1901 to 2010 (2.5° × 2.5° lat-long resolution) and National Centers for Environmental Prediction (NCEP)-National Center for Atmospheric Research (NCAR) Reanalysis Project (Kalnay *et al.*, 1996) from 1948 to 2010 (2.5° × 2.5° lat-long resolution)
- European Centre for Medium-Range Weather Forecasts (ECMWF): The ERA 40 (Uppala *et al.*, 2005) from 1959 to 2001 (2.5° × 2.5° lat-lon resolution) and ERA Interim (Dee *et al.*, 2011) from 1979 to 2010 (1.5° × 1.5° lat-lon resolution)
- Japanese 55-year Reanalysis (JRA-55) Project (Ebita *et al.*, 2011) from 1958 to 2010 (1.25 ° × 1.25° lat-lon resolution)

Table 2. Periods of available observed climate data from AEMET stations at the locations of study in the IP.

Locations	Periods	Missing years
Lugo	1986–2010	1990, 2001, and 2002
Lérida	1960–2010	1970, 1978, 1986, and 1990
Madrid	1960–2010	1969, 1970, 1971, 1983, and 1984
Albacete	1961–2010	1969, 1986, 1987, 1988, 1991, and 1998
Córdoba	1969–2010	1982, 1983, 1984, 1985, 1986, and 1991

Missing years are indicated.

The SST is taken from Reynolds SST dataset (ERSST, Smith *et al.*, 2008) and use to calculate El Niño index. In particular, El Niño3 index is chosen for the analysis

because it provides higher correlations than other Niño indices in a previous study (Capa-Morocho *et al.*, 2014). This is defined as the spatial average of the SST in the tropical Pacific area between 5°N–5°S and 90°–150°W. Seasonal indices based on the mean of three consecutive months of El Niño3, starting in January-February-March (JFM) and ending in December-January-February (DJF), are defined for calculating the lead correlations between El Niño and crop yield with the aim of assessing predictability.

2.4. Methodology and methods for variability analysis

The methodology comprises several steps: (1) to test the applicability of reanalysis data, (2) to generate longer time series of simulated potential maize yield, (3) to extract the high frequency component of simulated yield variability to focus on the interannual variability, (4) to determine the spatial pattern of yield variability that maximizes the variance of yield over IP, (5) to identify the climate variables among those used as inputs in the crop model with significant influence on yield, (6) to determine the spatial pattern that maximizes the variance of the climate variables over IP identified in the former step, (7) to identify relationships among El Niño3 index, simulated yield at each location, and the atmospheric variables with significant influence on yield, (8) to assess the stationarity of El Niño–yield and El Niño-climate variables (with significant influence on yield) relationship, (9) to study the atmospheric dynamical mechanism of the El Niño influences, and (10) to infer hypothesis about the eco-physiological mechanism behind crop response. The specific methods for each step are described below.

The applicability of the reanalysis datasets for the purposes of this study is tested by comparing the anomalies of the simulated crop yield done with reanalysis data with those obtained with observed weather data (AEMET).

Once the reliability of reanalysis datasets is verified, these are used to generate longer time series of simulated potential maize yield with CERES model. From these time series, the standard anomalies are calculated subtracting the mean value for each data and dividing it by the standard deviation. Afterwards, time series are time filtered to focus on the interannual variability. In this study, a ten-order low-pass butterworth filter (Butterworth, 1930; Roe and Steig, 2004) and cut off frequency of 0.2 (cut off frequency is $f = 2*\mathrm{d}t/T$, being $\mathrm{d}t = 1$, and $T = 10$ years) are used. Consequently, the original time series are split up in two components: low frequency (LF) and high frequency (HF) time scales (von Storch and Zwiers, 2001). While the HF varies at interannual time scales, the LF contains all variability with periods longer than 10 years.

HF time series of yield anomalies are used to study the spatial pattern of yield variability in IP. Thus, principal component analysis/empirical orthogonal functions [PCA/EOF (von Storch and Zwiers, 2001)] is used to determine the spatial pattern that maximizes the variance of yield over IP. The EOF analysis (EOF) discriminates the principal spatial directions in which the variance of a variable is maximized. To determine them, the time covariance matrix is computed: $\mathrm{Cov} = (1/(nt-1)) \times \boldsymbol{Y} \times \boldsymbol{Y}_t$, being $\boldsymbol{Y}$ a matrix of crop yield, $\boldsymbol{Y}_t$ the transpose of Y matrix, and nt the number of years considered in the analysis. The diagonalization is performed, being the EOFs the principal eigenvectors and the explained variance associated with each EOF the resultant normalized eigenvalues. In the time domain, the principal component (PC) are attached to the corresponding EOF, providing the amplitude score of each EOF spatial pattern for each time step, giving the simplified representation of the amplitude of the EOF along time (Hannachi, 2004).

Correlations analyses are used to identify the climate variables among those used as inputs in the crop model (T_{max}, T_{min}, Prec, Rad) with significant influence on yield (hereafter the climate variable with significant influences on yield are abbreviated with 'CVx'). For this purpose, the seasonal averages of the detrended climate variables corresponding to the crop cycle are used for this analysis: May-June-July (MJJ), June-July-August (JJA), and July-August-September (JAS). Afterwards, the same PCA is used to determine the spatial pattern that maximizes the variance of the 'CVx' variables over IP. The IP region is delimiting approximately from 35°to 45°N and from 11°W to 5.6°E.

Regression maps are used to identify relationships between El Niño3 index or the time series of simulated yield at each location, and the time series of climate variable anomalies (CVx) of each grid-point in IP. El Niño3 index corresponding to JAS is used because is the season when the grain filling takes places. Although regression analysis only reveals statistical relationships and it does not prove cause and effect, regression maps help to study the atmospheric mechanism of influences. These maps are computed projecting (1) the leading PC (PC1) of yield onto the 'CVx' at each grid-point, (2) El Niño3 of JAS onto the 'CVx' at each grid-point, and (3) El Niño3 of JAS onto the yield anomalies at each location. Those locations with significant correlations score between the time series of yield anomalies and El Niño3 index are highlighted in the regression maps.

To assess the stationarity of El Niño–yield and El Niño-CVx relationship, the leading PC (PC1s) of yield and CVx are used. Additionally, 21-year windows correlations scores, sliding 1 year, between the PC1s and the El Niño3 seasonal index before the harvest date are calculated. Seasonal indices based on the mean of three consecutive months El Niño3, starting in January-February-March (JFM) and ending in December-January-February (DJF), are defined for calculating the lead correlations between El Niño and yield anomalies. Windows of 21 years are chosen for this analysis because this value has been used in El Niño-Southern Oscillation (ENSO) impacts on atmospheric variables over Europe (Lorenzo *et al.*, 2011; López-Parages and Rodríguez-Fonseca, 2012). Thus, correlations are calculated for the period that starts on January-February-March in the year previous to sowing (hereafter JFM-L, the L coming from previous year, or lag year) and finishes on July-August-September (JAS) in the same year that harvest takes place.

To study the atmospheric dynamical mechanism of the El Niño influences and to infer hypothesis about the eco-physiological mechanism behind crop response, a period with significant influences of El Niño in IP is chosen. Consequently, in this period, correlations maps between the PC1 of yield variability in IP and SST for the spring and summer seasons corresponding to the year before crop cycle (AMJ-L, JAS-L) and to the year of crop cycle (AMJ, JAS) are computed. Also, regressions maps among the 400 hPa geopotential height anomalies in Europe for JAS and the PC1 of yield variability in IP, and El Niño3 index for JAS are computed. The European region is delimiting approximately from 30° to 70°N and from 20°W to 40°E. These maps are obtained projecting (1) the CVx anomalies at each grid-point throughout the Europe for JAS onto PC1 of yield variability in IP, (2) the 400 hPa geopotential height anomalies (Z400) of each grid-point throughout the Europe onto PC1 of yield variability in IP, and (3) the 400 hPa geopotential height anomalies (Z400) at each grid-point throughout the Europe onto Niño3-JAS. The atmospheric variables are considered from the reanalysis data set used to run the crop model in each of the cases. Statistical significant areas with significant correlations scores between the anomalies time series and PC1 or El Niño3 index are highlighted in the regression maps.

MATLAB software is used for all the analyses. Throughout the study, a 95% confidence level of significance, which is determined by a non-parametric Monte Carlo test with 100 permutations, is used when is not specified.

3. Results

3.1. Crop simulations with observed weather data *versus* reanalysis data

Time series of simulated yield obtained at each location with both reanalysis and observed data show similar evolution of the anomalies (Figure 2). Some decades exhibit stronger variability than others, with some decadal modulations in the amplitude. In this way, for the second half of the past century, the yield variability at higher frequencies is stronger than in the first half of the century, reaching absolute values of the anomalies higher than two standard deviations at all locations after the 1950's. Also, decadal variability is noticed in the evolution of the time series.

Extended simulated series of crop yield anomalies using different reanalyses datasets show a significant agreement with simulated yield using observed climate at all locations for the available years. The best agreement corresponded to ERA Interim dataset (Table 3), reaching values of correlation of 0.82 in Lugo. Significant agreement is found between yield anomalies simulated with different reanalyses data at all locations (Figure 3), being the best agreement between ERA 40 and ERA interim reanalyses (with correlation values higher than 0.79). The highest correlation values are obtained in the North of the IP (Lugo and Lérida). Only southern locations (Albacete and Córdoba) show two cases of no significant agreement between yield simulated with 20th Century and some reanalyses datasets. For instance, in Albacete (SE region), yield anomalies simulated with 20th Century datasets are not significantly correlated with those simulated with NCEP and ERA Interim. Meanwhile, in Córdoba (South region), yield anomalies simulated with 20th Century datasets are not significantly correlated with yield anomalies simulated with JRA-55 and ERA 40.

3.2. Leading mode of yield variability and temperature in IP

The analyses of the spatial distribution of IP yield variability, computed using different reanalysis datasets, exhibit a leading mode that is clearly separated from the second one. The leading mode explains *ca* 50% of the total variance of yield in IP (Table 4). Regarding the time evolution of the pattern, the amplitude of the standardized leading PC (PC1s) is not stationary over time (Figure 4(a)): the time series of standardized PC1s show that yield variability associated with the leading mode was lower during the first part of the last century (from 1912 to 1950) than that of the rest of the century, up to the 1990's.

The first EOF (EOF1s) of yield in IP (Figure 4(b)) computed using the longest reanalyses datasets (20th Century and NCEP, with 110 and 63 years, respectively) show a similar behaviour of yield through IP, appearing the highest values of yield anomalies in the northern region. This means that in the years with positive values (weight) in the PC1, the yield would increase throughout the IP appearing larger yield anomalies in the northern locations than in the southern ones. Meanwhile, for the years with negative values (weight) in the PC1, the yield would decrease throughout the IP appearing smaller yield anomalies in the northern locations than in the southern ones.

EOF1s computed using shorter data reanalysis (JRA-55, ERA 40, and ERA Interim reanalysis, with 53, 43 and 32 years, respectively) show a dipolar pattern of yield behaviour: a centre of yield anomalies over southern region with opposite behaviour than the centre of yield anomalies over the North and centre of IP. This means that for years with positive values in the PC1, the yield decrease in the southern location and the yield increases in the remaining locations, and vice versa for years with negative values in the PC1 (increase in the southern location and decrease in the remaining locations). However, the correlation between the low centre over the southern region and their PC1 [shown in small circles Figure 4(b)] is no significant, except when using the ERA Interim dataset. It suggests that for the last decades, between 1980 and 2010, there was a dipole behaviour of yield in IP, indicating a possible non-stationarity of the yield variability pattern, if the reliability of the different reanalysis is assumed.

The climate variables used as inputs in the crop model during the growing season with the strongest impact on yield variability are identified. In most locations, the climate variables with the strongest impact on yield variability are maximum and minimum temperatures (T_{max},

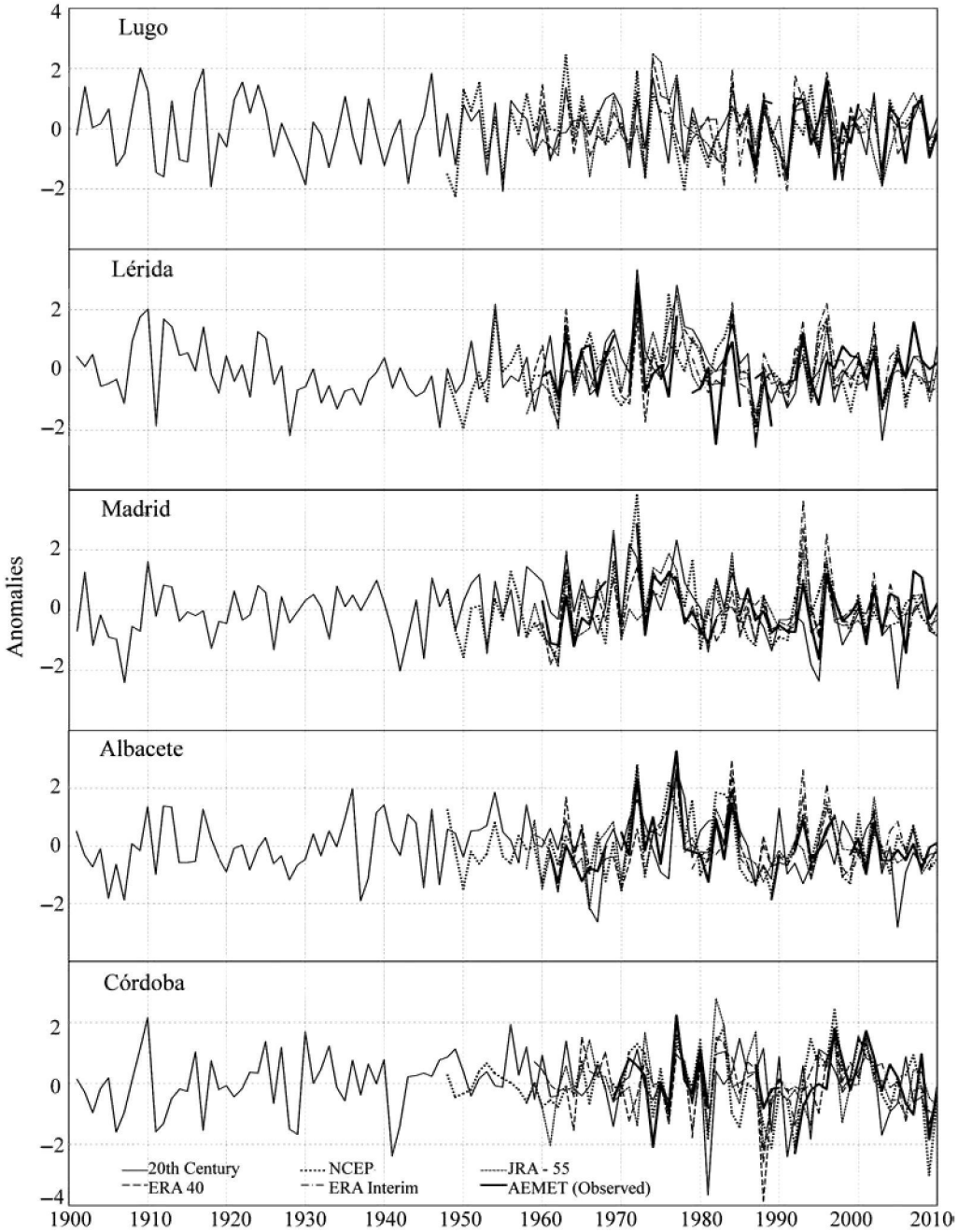

Figure 2. Maize yield anomalies by location. Standardized anomalies of crop yield obtained from simulations performed with observed (AEMET) and all global reanalyses atmospheric datasets (20th Century, NCEP, JRA-55, ERA 40, ERA Interim) at five locations in IP (Figure 1). The simulation periods correspond to the extent of the corresponding datasets.

T_{min}) in July-August-September (JAS, Table 5). This period is the expected one as JAS roughly coincides with the maize grain filling period in IP. The yield anomalies are negatively correlated to T_{max} and T_{min} of JAS at all locations, and all correlations are significant at all locations but Córdoba (Table 5), where they are significant only for 20th Century, NCEP, and ERA Interim. Therefore, the yield increases when T_{max}, T_{min} in JAS decreases, and vice versa (yield decreases when T_{max}, T_{min} increases). The crop model calculates the mean temperature (T_{mean}) from T_{max} and T_{min} used as input, because T_{mean} is used to compute the thermal time, which causes crop development to progress from one phenostage to another. Therefore, there is also an influence of T_{mean} and it is included in the analysis.

Thus, considering only temperatures, the spatial pattern that maximizes the variance of T_{max}, T_{min}, and T_{mean} in JAS in IP is determined. The EOF analysis obtains a leading mode (pattern) of temperature variability that explains over 50% of the total variance of temperature throughout the IP (Table 4). Figure 5 shows the result of regressing the respective leading PC (PC1) of IP temperature anomalies (T_{max}, T_{min}, and T_{mean}) onto each of the temperature field, in order to characterize the spatial pattern

Table 3. Performance of reanalyses datasets in generating simulated yield anomalies.

Location	Reanalyses dataset				
	20th Century	NCEP	JRA 55	ERA 40	ERA Interim
Lugo	**0.63**	**0.58**	**0.59**	0.50[a]	**0.82**
n	22	22	22	14	22
Lérida	**0.59**	**0.31**	**0.53**	**0.44**	0.31[a]
n	47	47	47	38	30
Madrid	**0.54**	**0.57**	**0.60**	**0.70**	**0.72**
n	46	46	46	37	30
Albacete	**0.43**	**0.61**	**0.78**	**0.63**	**0.71**
n	44	44	44	35	27
Córdoba	**0.46**	**0.71**	**0.46**	**0.46**	**0.68**
n	36	36	36	27	26

Correlations between standardized yield anomalies simulated with inputs from observed weather data (AEMET) and those anomalies simulated with several atmospheric reanalyses datasets (20 Century, NCEP, JRA-55, ERA 40 and ERA Interim), for the period corresponding to the available observations at each location (*n* is the number of years). Statistical significant correlations (significance level $p < 0.05$) are set in boldface. [a]Significant levels > 90%.

of the EOF. These regression maps represent the amplitude of changes in temperatures: a positive structure of temperature anomalies over all IP, with the maximum anomalies over NE region. This means that the years with positive (negative) weight in the PC1 of temperature in IP are associated with warmer (cooler) temperatures than normal ones (T_{max}, T_{min}, T_{mean}) through IP. All reanalyses datasets used for the analysis show the same pattern of temperature variability with the centre of higher variations in the same region but with different intensity; the greatest temperature variability is observed in the T_{max}. In addition, the highest (intensity) temperature variability is found using reanalyses data from NOAA.

Comparing the leading temperature variability pattern (Figure 5) with the leading yield variability pattern (Figure 4(b)), it is shown how the centre of higher variability for both temperature and yield is the northern region of the IP.

3.3. Relationships between yield, temperature, and El Niño index: stationarity

Taking into account the relation found in Capa-Morocho *et al.* (2014) between El Niño and anomalies yield in Lugo, the influence of El Niño is analysed for the whole IP. Considering all the available periods of reanalyses datasets (ranging from 32 to 110 years), the regression maps between (1) the leading PC of yield and T_{mean}, (2) T_{mean} anomalies and El Niño3 index, and (3) El Niño3 index and anomalies yield are represented in Figure 6. In this way, a mechanism linking yield variability and El Niño can be found through El Niño influence on T_{mean}. Results of regression between PC1 of yield variability in IP and T_{mean} anomalies at grid points in IP for JAS (Figure 6(a)) show the same spatial pattern of relationship with all datasets used and therefore for all available periods. This spatial pattern indicates that the PC1 of yield

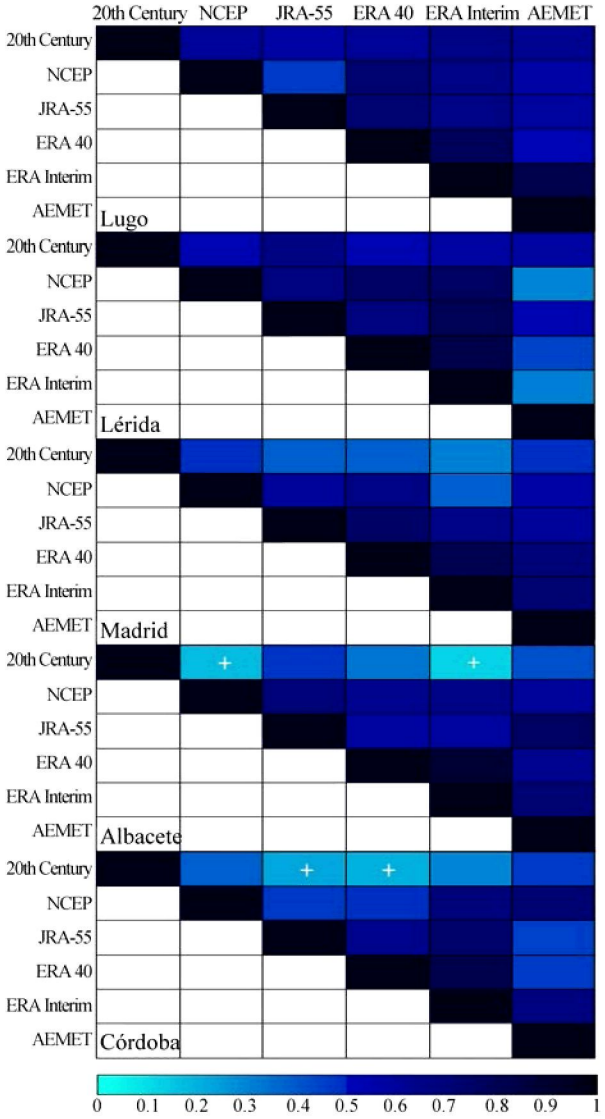

Figure 3. Correlations between the time series of yield anomalies simulated with several datasets (reanalyses and AEMET observations). No statistical significant correlations are indicated with crosses.

is negatively associated with the T_{mean} anomalies at grid points in IP. This suggests that the T_{mean}–yield relationship is stationary over the time. This means that yield increases in IP when the T_{mean} decreases in IP whatever the period. In contrast, when T_{mean} increases the yield decreases. The highest variations in both yield and temperature appear in the NE of IP. This spatial pattern indicates that there are higher influences of temperatures on yield in the northern region than in the rest of IP. Moreover, the spatial regression pattern between T_{mean} and the PC1 of yield presents a similar pattern that the EOF1 of T_{mean} in JAS (Figure 5(c)), with the maximum values over NE region. This is confirmed by the significant correlation of the PC1s of temperatures with the PC1s of yield over IP (Table 6), with correlation values ranging between −0.64 and −0.84.

Moreover, taking into account all the available periods of reanalyses datasets, results of regression between El Niño3 and T_{mean} anomalies at each grid-point of IP (Figure 6(b)) and regression between El Niño3 and yield

Table 4. Explained variance (%) of the leading mode of the yield anomalies at IP and of the atmospheric variables of JAS at IP.

PC1	Reanalyses dataset				
	20th Century	NCEP	JRA-55	ERA40	ERA Interim
Yield	47.65	50.99	51.61	57.23	59.71
T_{max}	60.96	62.03	65.21	62.25	57.98
T_{min}	63.17	58.56	66.80	65.52	64.28
T_{mean}	63.93	63.39	66.87	65.52	62.09
Rad	46.08	39.89	25.10	41.04	34.88
Prec	37.60	44.77	37.69	31.88	27.38

anomalies at each location of IP (Figure 6(c)) show that El Niño3 index is not always significantly associated with both T_{mean} or yield, whatever period and location in IP (Figure 6(b) and (c)). Only some areas (Figure 6(b)) or locations (Figure 6(c)) and some reanalyses show significant influences of El Niño [shaded areas in Figure 6(b) and big dots and circles in Figure 6(c)]. This result suggests the non-stationary behaviour of El Niño on its influence over IP atmospheric variables and yield, in a way that, when using long time series, the relation could be opposite for some sub-periods and, thus, could be compensated when doing the regression. For this reason, when using shorter time series, the relation is stronger in some areas.

To check the stationarity of El Niño influence on yield further, 21-year window moving correlations between (1) PC1s of yield and El Niño3 and (2) PC1s of T_{mean} in IP for JAS and El Niño3 are computed for the different available reanalyses datasets (Figure 7). Results reveal important changes in the correlations during the second half of the 20th century, especially during the summers when the crop is growing and the SSTs from the previous year. The evolution of these correlations exhibits a clear multidecadal modulation for both yield and T_{mean} (Figure 7), and there is a consensus among all reanalysis datasets used. An opposite effect of El Niño phenomenon is observed on the yield in IP (Figure 7(a)) and the T_{mean} in IP (Figure 7(b)) throughout the whole century. At the beginning of the century (i.e. just before 1940) and after 1980s, a positive correlation between PC1 of yield (Figure 7(a)) and El Niño3 for the year previous to the crop cycle is found, whereas this correlation is negative for El Niño corresponding the

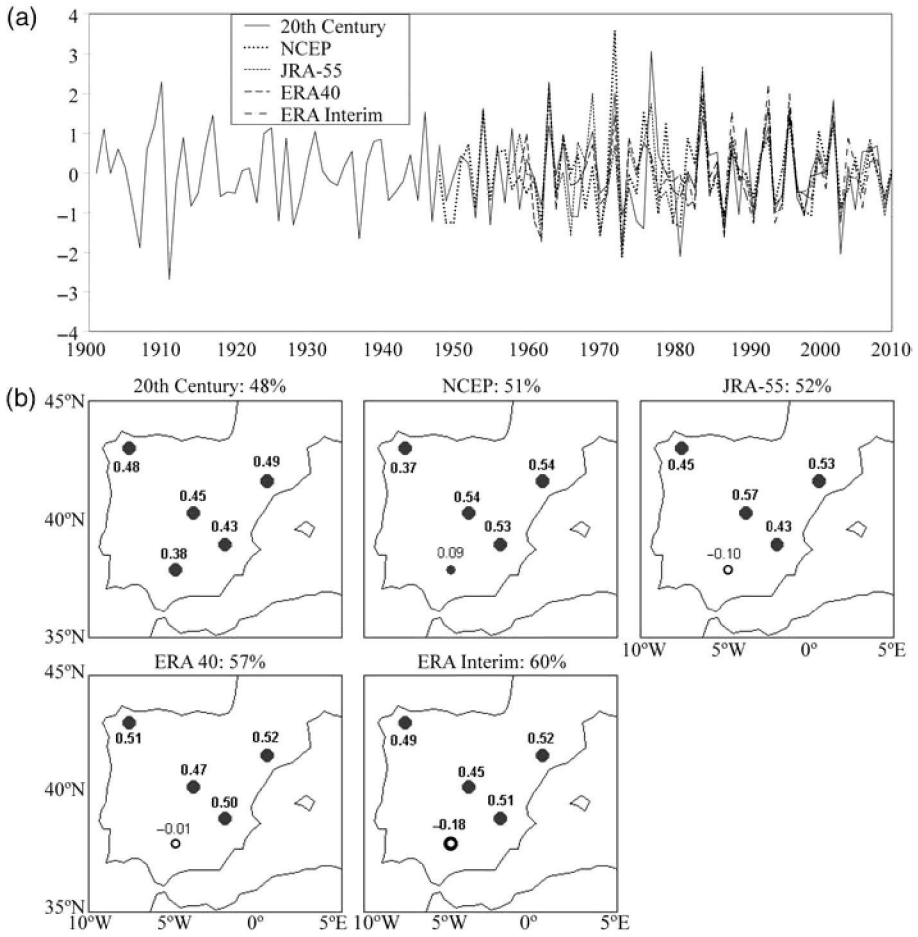

Figure 4. Leading mode of yield variability. (a) Standardized leading principal component (PC1) of simulated yield anomalies in IP. These time series represent the weights along time of the yield anomalous pattern associated with their respective EOF. (b) Leading empirical orthogonal functions (EOF1) of simulated yield at five locations in IP. The numbers are the yield anomalies at each location per standard deviation in the PC1. Each plot corresponds to crop simulations performed with a different reanalysis dataset. The value in the top of each figure represents the explained variance associated with EOF1. In the EOF figures, locations with positive correlations between the PC1 and the time series of yield anomalies are showed in dots and locations with negative correlations are showed in circles. Locations with significant correlation are set in boldface and big dots and circles.

Table 5. Correlations between yield simulated with several atmospheric reanalyses datasets (20 Century, NCEP, JRA-55, ERA 40 and ERA Interim) and reanalysis variables of July-August-September (JAS) used as inputs in crop model (T_{max}, T_{min}, Rad, Prec) for the period available of each reanalyses (n is the number of years).

Reanalysis (n)	Climate variables			
Location	T_{max}	T_{min}	Rad	Prec
20th Century (110)				
Lugo	**−0.52**	**−0.56**	−0.16	0.10
Lérida	**−0.31**	**−0.57**	**0.20**	**−0.28**
Madrid	**−0.68**	**−0.71**	0.01	0.07
Albacete	**−0.46**	**−0.52**	0.07	−0.03
Córdoba	**−0.28**	**−0.35**	**0.19**	−0.15
NCEP (63)				
Lugo	**−0.65**	**−0.71**	0.06	−0.05
Lérida	**−0.68**	**−0.66**	0.06	0.06
Madrid	**−0.66**	**−0.63**	−0.13	0.07
Albacete	**−0.41**	**−0.58**	0.08	0.01
Córdoba	**−0.40**	**−0.46**	0.07	0.02
JRA-55 (53)				
Lugo	**−0.50**	**−0.60**	0.12	0.05
Lérida	**−0.80**	**−0.88**	**−0.35**	**0.37**
Madrid	**−0.62**	**−0.74**	**−0.34**	**0.31**
Albacete	**−0.68**	**−0.70**	−0.12	**0.45**
Córdoba	−0.24	−0.27	0.14	−0.02
ERA 40 (43)				
Lugo	**−0.55**	**−0.64**	−0.10	0.04
Lérida	**−0.71**	**−0.76**	−0.17	0.28
Madrid	**−0.76**	**−0.73**	−0.19	0.23
Albacete	**−0.72**	**−0.74**	0.01	0.02
Córdoba	−0.25	−0.24	0.05	−0.01
ERA Interim (32)				
Lugo	**−0.62**	**−0.71**	0.06	−0.07
Lérida	**−0.69**	**−0.79**	0.26	**−0.36**
Madrid	**−0.63**	**−0.64**	0.01	−0.14
Albacete	**−0.74**	**−0.77**	0.10	−0.09
Córdoba	**−0.45**	**−0.36**	−0.18	0.16

Statistical significant correlations (significance level $p < 0.05$) are set in boldface.

crop cycle year. In contrast, the correlation between PC1 of T_{mean} and El Niño3 is negative for previous seasons to crop cycle and positive for those El Niño indexes corresponding to crop cycle (Figure 7(b)). However, between the 1960 and 1980, the yield and T_{mean} correlations are opposite to the relationships listed above: for instance, the PC1 of yield had a negative correlation with El Niño3 for the previous seasons to the crop cycle and positive for the El Niño3 of the year when the crop cycle takes place. Therefore, this would suggest that both high yield anomalies and low T_{mean} anomalies can be associated with transitions of the El Niño-to-La Niña or the La Niña-to-El Niño depending on the period. Consequently, there may be an opposite relationship between El Niño–yield anomalies and El Niño–T_{mean} anomalies, and the influences of El Niño on yield and T_{mean} are no stationary. This result agrees with López-Parages and Rodríguez-Fonseca (2012) in which opposite teleconnection pattern is found in the Euro Mediterranean atmospheric variability as a response to an El Niño depending on the time period considered. More recently López-Parages *et al.* (2014) have posed a possible dynamical mechanism that could explain why ENSO teleconnections with Europe can be or not effective and how the internal multidecadal variability of the coupled atmosphere–ocean system can play an important role.

3.4. Atmospheric mechanism and teleconnection

The period with the stronger influence of El Niño on the leading mode of yield variability and also on the JAS T_{mean} in IP is 1960–1980 (Figure 7). For 1960–1980, the correlation map between the PC1 of yield in IP and SST anomalies in the tropical region for AMJ-L, JAS-L AMJ, and JAS seasons resemble a transition between La Niña pattern and El Niño pattern over the Pacific (Figure 8), because there are significant changes in the correlations during the spring–summer seasons of both: the year previous to crop cycle and the year of crop cycle. Therefore, during these decades, high yield anomalies in IP are associated with La Niña-El Niño transitions and low yield anomalies are associated with El Niño-La Niña transitions. This is a novel result, as previous works done by López-Parages and Rodríguez-Fonseca (2012) and López-Parages *et al.* (2014) do not consider lag in the analysis.

To analyse the relationship between PC1 of yield in IP and T_{mean} anomalies in Europe, it is important to characterize the atmospheric anomalous patterns that is related to El Niño and how it can influence on T_{mean}. In this way, (1) PC1 of yield and 400 hPa geopotential height (Z400) anomalies and (2) El Niño and Z400 are presented in Figure 9 for the 1960–1980 period and JAS season. This level (400 hPa) is representative of the middle troposphere and it is the closest available level (common to all reanalyses) to the one for which the north Atlantic teleconnection patterns are defined (500 hPa). The results show a similar dipolar structure for the different regression maps done with the PC1 of yield and reanalysis (Figure 9(a) and (b)): a centre of action which spans IP and western-Mediterranean opposite in sign to the centre of action which spans Scandinavia and northeastern Europe. The regression maps indicate that positive yield anomalies in IP are associated with both negative T_{mean} anomalies in IP and positive T_{mean} anomalies in Scandinavia and northeastern Europe, and vice versa for negative yield anomalies. Besides, a similar spatial pattern of regression appears between PC1 of maize yield in IP and Z400 anomalies in Europe (Figure 9(b)). This means that positive yield anomalies in IP are associated with both negative geopotential height anomalies in IP and positive geopotential height anomalies in Scandinavia and northeastern Europe. The atmospheric pattern is part of a large scale pattern (not shown) coming from the Pacific and obtained in López-Parages *et al.* (2014). This configuration resembled Scandinavian pattern in positive phase, which is associated with positive height anomalies over Scandinavian Peninsula (Bueh and Nakamura, 2007; CPC: Climate Prediction Center, 2012). Moreover, the correlations between the Scandinavian index for JAS and the PC1 of yield in

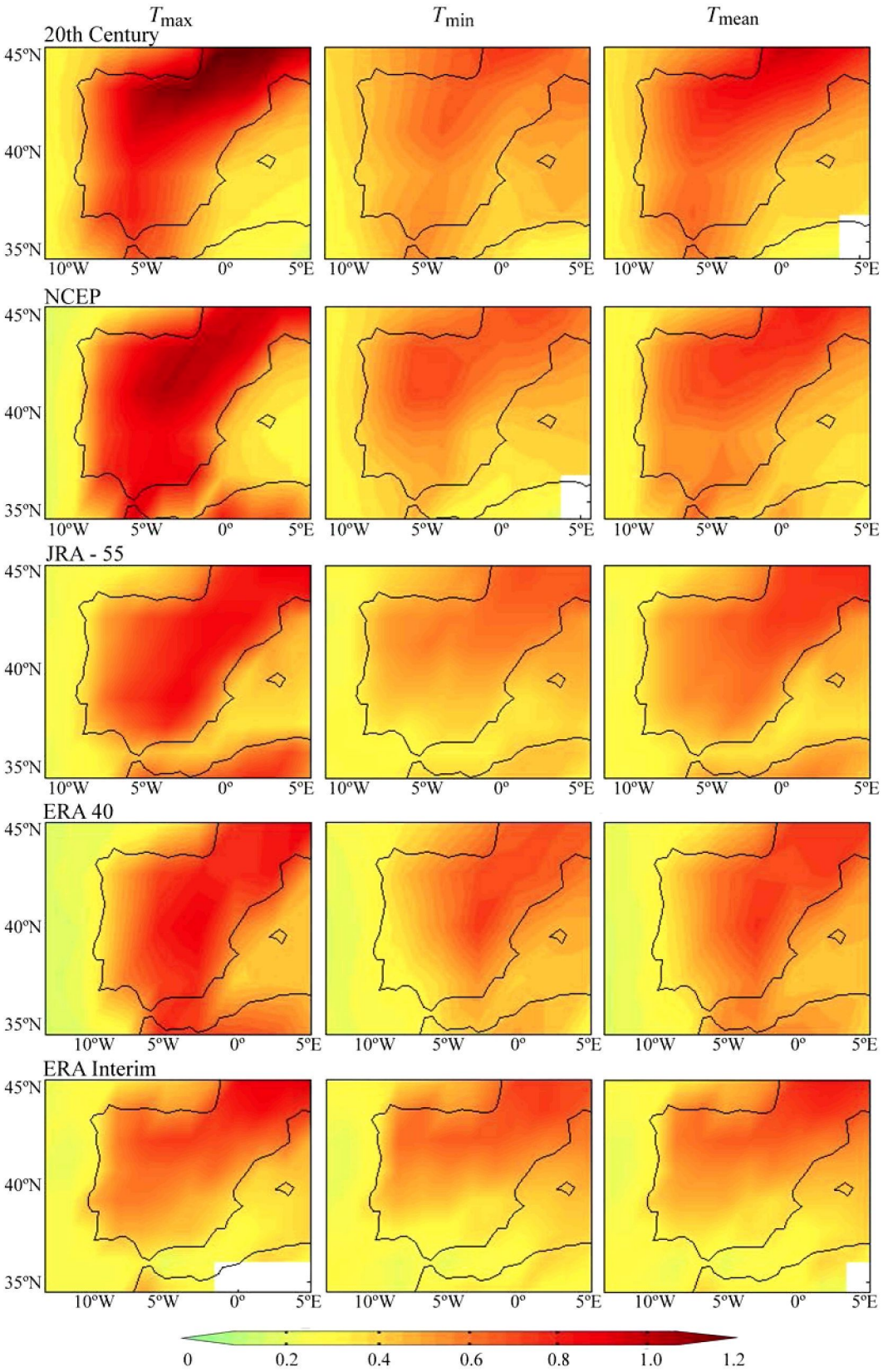

Figure 5. Leading mode of temperature variability over IP. Regression maps between temperature anomalies (T_{max}, T_{min}, and T_{mean}) at each of the spatial grid points and PC1 of T_{max}, T_{min}, and T_{mean} during JAS for different reanalysis datasets (°C per SD in the PC1 of temperature anomalies in IP). Statistical significant areas, according to a Monte Carlo correlation test at 95% confidence level, are shaded.

Table 6. Correlation between PC1 of simulated yield and PC1 of atmospheric variables during JAS over IP.

Climate variables	Reanalyses dataset				
	20th Century	NCEP	JRA55	ERA 40	ERA Interim
T_{max}	**−0.72**	**−0.70**	**−0.71**	**−0.78**	**−0.79**
T_{min}	**−0.76**	**−0.65**	**−0.64**	**−0.75**	**−0.84**
T_{mean}	**−0.75**	**−0.73**	**−0.70**	**−0.80**	**−0.83**
Rad	**−0.46**	−0.15	−0.26	−0.23	0.10
Prec	−0.05	0.13	0.27	0.27	0.16

Statistical significant correlations (confidence level $p < 0.05$) are set in boldface.

IP are significantly positive using NCEP (0.39), JRA-55 (0.45), and ERA 40 (maximum value, 0.52). This means that positive yield anomalies in the IP are associated with a positive phase of Scandinavian pattern and vice versa for negative yield anomalies.

The spatial pattern of regression between El Niño3 and Z400 anomalies in Europe (Figure 9(c)) presents a similar dipolar structure than the Z400 anomalies-PC1 yield relationship: a negative centre of action over IP and a weak positive centre of action over the North of Europe, being only significant in IP region. This configuration also resembles the Scandinavian pattern in positive phases. Consequently, this suggests that El Niño events are associated with a positive phase of Scandinavian pattern, which exerts an influence on T_{mean} and, thus, on the crop yield in IP. Therefore, there is an evidence of the atmospheric response to El Niño over Europe, which affects the geopotential height patterns, and in turn affects minimum and maximum temperature in IP, and finally influences on maize yield variability.

4. Discussion

In this study, we have used a site-specific calibrated and validated crop model and a number of atmospheric reanalysis datasets to generate long time series of simulated potential yield. Observed field (crop) data were only used here to calibrate and validate the crop model, as our study relies on the simulated potential yield as a mean to isolate climate influence. We have found a good agreement between simulated yields with observed weather data and those obtained with the reanalysis datasets. Consequently, the evidence from this study suggests that simulations done with reanalyses could be used as an alternative methodology to obtain long time series of potential yield. This allows us to explore associations between maize yield anomalies in IP and SST anomalies in the past. In some locations, the correlations between 20th Century dataset and the remaining reanalysis datasets (NCEP, JRA-55, ERA 40, and ERA Interim) show low values, probably because the 20th Century dataset uses only surface pressure reports, observed monthly SST and sea-ice distributions as boundary conditions (Compo *et al.*, 2011). Meanwhile, the rest of reanalyses used here consider more data in the assimilation process: i.e. snow, albedo, soil wetness, and vegetation resistance (Kalnay *et al.*, 1996). Nevertheless, the use of 20th Century datasets is reasonable because our interest is in the role of SST variability on the leading PC of yield and this reanalysis has been developed assimilating observed SST along the 20th century. For this reason, the lower correlations that we obtain appear in those locations where the SST variability does not determine the changes in the yield. It is the case of Cordoba, where the SST is not related with the leading PC of yield (Figure 4), or at Albacete where it has been compared with a reanalysis (ERA Interim) that spans a period that does not present a relation with El Niño. Except for NCEP in Albacete (Figure 3), the rest of reanalysis present significant correlation with 20th century. Thus, the yield evolution along the 20th century obtained simulating with the 20th Century reanalysis offers some understanding on the decadal variability and modulations of crop yield in IP along the 20th century. This study was conducted for an irrigated crop; however, some limitations appear in the use of reanalysis precipitation data for rain-fed crop simulations with active soil water dynamics. The spatially averaged precipitation at low resolution, which is interpreted by the crop model as point data, can lead to odd responses (Capa-Morocho *et al.*, 2014).

This study has found how most of the variability of maize yield in Spain can be explained by a homogeneous pattern with the same behaviour through the peninsula. We have found a stronger association between El Niño and the leading mode of variability of maize yield in IP than the previously reported one (Gimeno *et al.*, 2002), probably due to the use of potential yield instead of historical and statistical yields, which were affected by other factors than weather. For instance, Gimeno *et al.* (2002) characterized the empirical influence of ENSO on the main Spanish crops using historical yield data from Food and Agriculture Organization (FAO) records, obtaining a weak response to ENSO phases, and being only significant for lemon and tangerines yields. The use of potential yield has allowed us to isolate the influence of the main environmental variables in irrigated summer crops: daily solar radiation and maximum and minimum temperature.

Nevertheless, the relation between maize yield and El Niño found here is non-stationary, which means that it does not hold on during the whole record, confirming the El Niño–yield relationship found by Capa-Morocho *et al.* (2014) in the NW of IP. Our results show also an agreement with the studies showing multidecadal changes in the impact of ENSO on climate variables

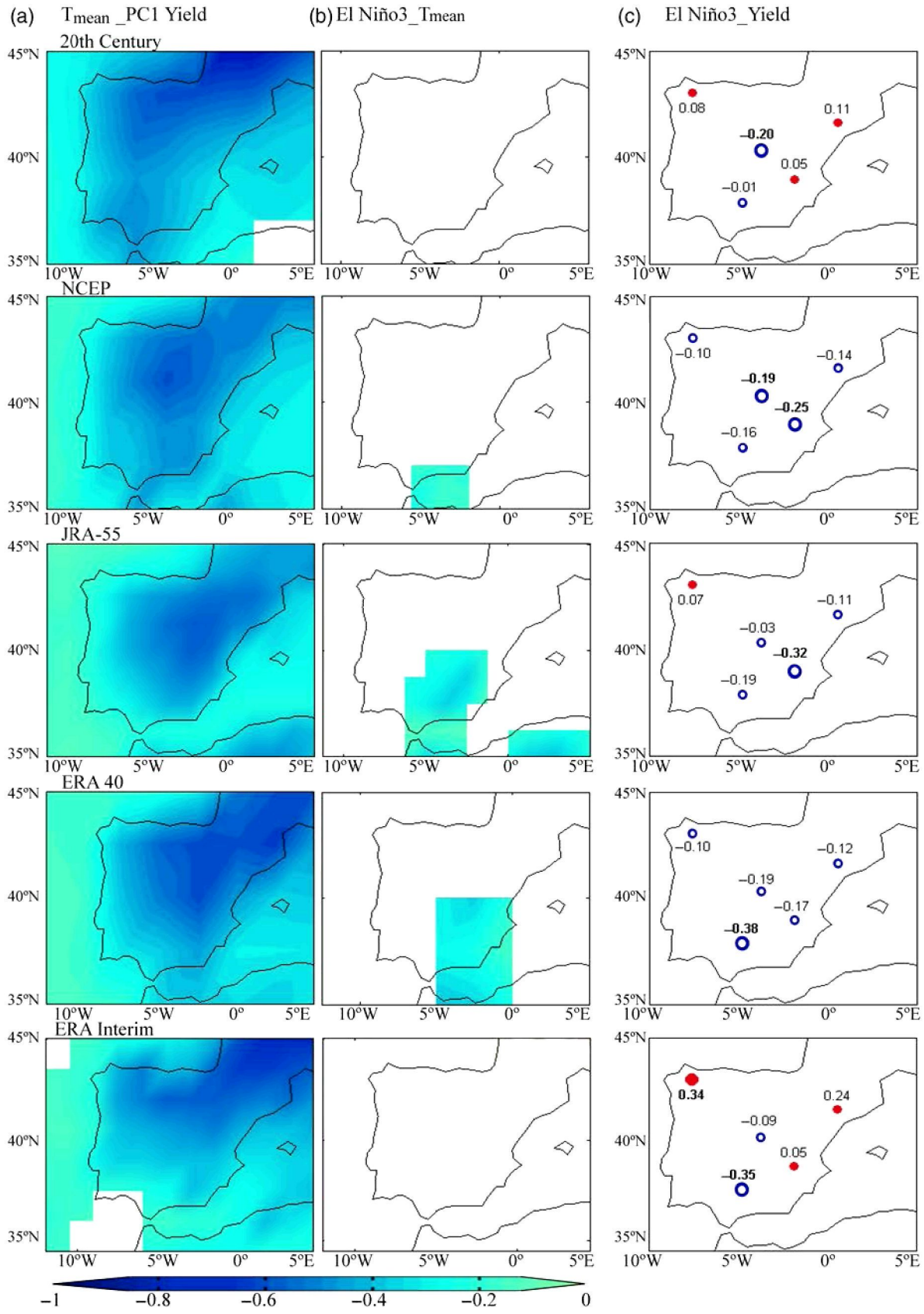

Figure 6. Spatial regression maps obtained projecting (a) PC1 of yield variability in IP onto T_{mean} anomalies at grid points of IP for JAS (°C per SD in the PC1 of yield anomalies). (b) El Niño3 index onto T_{mean} anomalies at grid points of IP for JAS (°C per SD in the El Niño3 index). Statistical significant areas, according to a Monte Carlo test at 95% confidence level, are shaded. (c) El Niño3 for JAS onto yield anomalies at each location (yield anomalies per SD in the El Niño3 index). Locations with positive correlations between yield anomalies and El Niño3 are showed in dots and locations with negative correlations are showed in circles. Locations with significant correlation are set in boldface and big dots and circles.

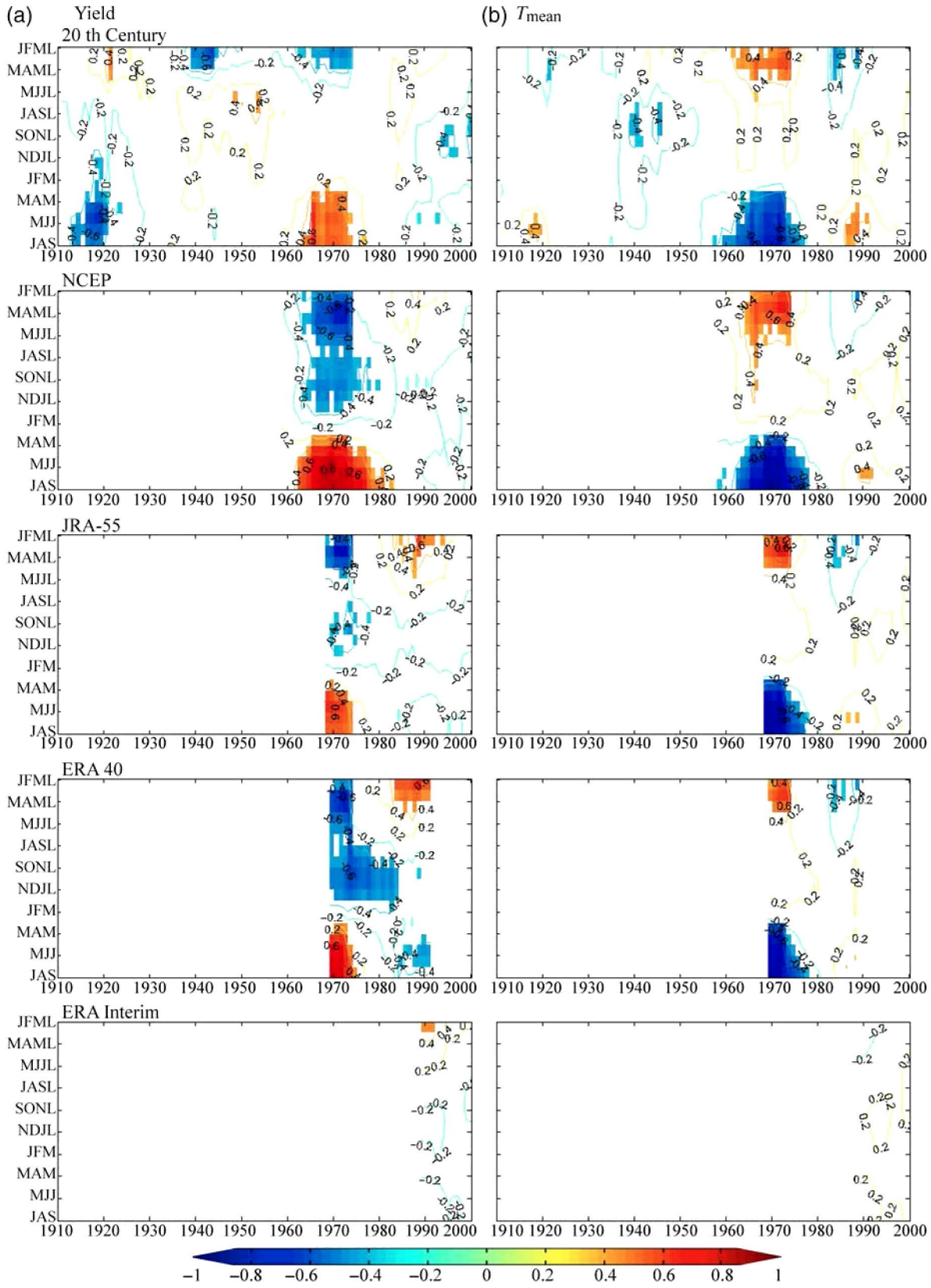

Figure 7. Stationarity of the El Niño–yield and El Niño–T_{mean} relationships. Twenty-one year moving window correlations (sliding 1 year) between (a) PC1 of yield anomalies in IP (simulated with several reanalyses datasets) and El Niño3 for seasons before the harvest date (from January–February–March of the year preceding the harvest year or lag season, L ('JFM-L'), to July–August–September of the crop cycle year ('JAS'). (b) The same as (a) but with PC1 of JAS T_{mean} anomalies. The x-axis represents the midpoint of the 21-year windows for which correlation is calculated, and the y-axis shows the El Niño season. The shaded areas show periods with 95% significant correlations according to a Monte Carlo test. Each plot corresponds to crop simulations performed with a different reanalysis dataset.

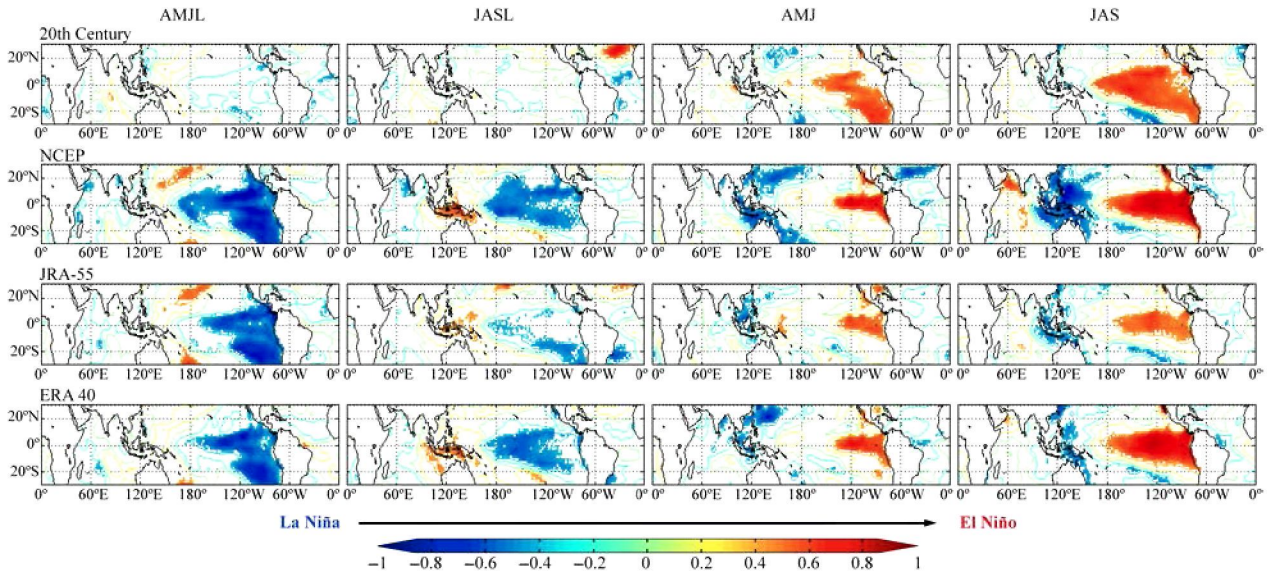

Figure 8. Spatial distribution of the correlation between seasonal anomalous SST (corresponding to 1 year before the crop season: AMJ-L, JAS-L, and to the cropping year: AMJ, JAS) and the PC1 of maize yield anomalies for 1960–1980. Statistical significant areas, according to a Monte Carlo correlation test at 95% confidence level, are shaded.

in Europe (Diaz *et al.*, 2001; Mariotti *et al.*, 2002; Knippertz *et al.*, 2003; Greatbatch *et al.*, 2004; Brönnimann, 2007; López-Parages and Rodríguez-Fonseca, 2012). This non-stationarity may help to explain why the El Niño–yield relationships were weak when the study period was long, due to the compensations pointed in the results section. Moreover, multidecadal changes in the impact of ENSO in Europe seem to be modulated by multidecadal patterns, such as Atlantic Multidecadal Oscillation (AMO) and Interdecadal Pacific Oscillation (IPO) (Zanchettin *et al.*, 2008; López-Parages and Rodríguez-Fonseca, 2012). López-Parages and Rodríguez-Fonseca (2012) show that under negative phases of the AMO, the general circulation of the atmosphere favours the Rossby wave propagation that are originated by anomalous divergence in the Equatorial Pacific, which in turn is triggered by El Niño. Nevertheless, when the AMO is in positive phases there is not ENSO teleconnection. This result is in agreement with ours, as we have found an enhancement of ENSO influence on yield on AMO negative periods. This fact would open a window of opportunity of crop yields predictability under negative phase of AMO. Nevertheless, further analysis is needed to verify this hypothesis.

The highest correlations with the PC1 of yield in IP were found for El Niño3 of JAS, season where grain filling takes place. On the other hand, there was a significant correlation with El Niño3 index of 1 year in advance, being the best predictors El Niño3 index corresponding to the spring (AMJ-L) or summer (JAS-L) seasons of the year before the crop cycle. This suggests that yields of summer crops in IP could be influenced by either the preceding or/and the simultaneous phase of El Niño regarding the crop cycle. This kind of relationship has been also detected in other regions of the world. For instance, Handler (1990) found a significant correlation between SST anomalies in the eastern Pacific at varying lag time and state averaged yields of maize throughout the continental United States; specifically, a negative correlation ($r < -0.35$) with SSTs for the preceding winter (DJFL) to the growing season and a positive correlation ($r > 0.35$) with SSTs for the subsequent fall (SON) were found. Moreover, several authors invoke a lag in ENSO-European precipitation relationships (Rodó *et al.*, 1997; Van Oldenborgh *et al.*, 2000; Mariotti *et al.*, 2002; Bulic and Kucharski, 2012). The highest correlations between El Niño and PC1 of maize yield in IP have been found for the period 1960–1980, in agreement with Rozas and Garcia-Gonzalez (2012), who found a significant correlation with ENSO and oak latewood growth in Norwest IP during the period 1952–1980. Also, Rodó *et al.* (1997) found that the correlation between ENSO and Iberian rainfall has increased towards the end of the last century, maybe because El Niño phenomenon was registered more frequently and there were more transitions between the different events during the second half of that century. When we focus on the period 1960–1980, the relationship between El Niño (index of the crop cycle) and PC1 yield is consistent throughout the whole IP: low yields are associated with a La Niña event and the high yields are associated with an El Niño event. El Niño–yield association is weak only at the Southern locations. In other parts of the world, the same El Niño–maize yield relationship has been reported. For instance, Cadson *et al.* (1996) showed that maize yield in the Midwest of the United States tended to be higher during an El Niño (summer months) and lower during La Niña (summer months). They attributed the effect of El Niño (La Niña) event on maize yield to more (less) precipitation in July, August, and September and low (high) temperatures.

The influences of the El Niño phenomenon on summer crop yield could be explained by the ocean surface thermodynamic effect on the atmospheric circulation,

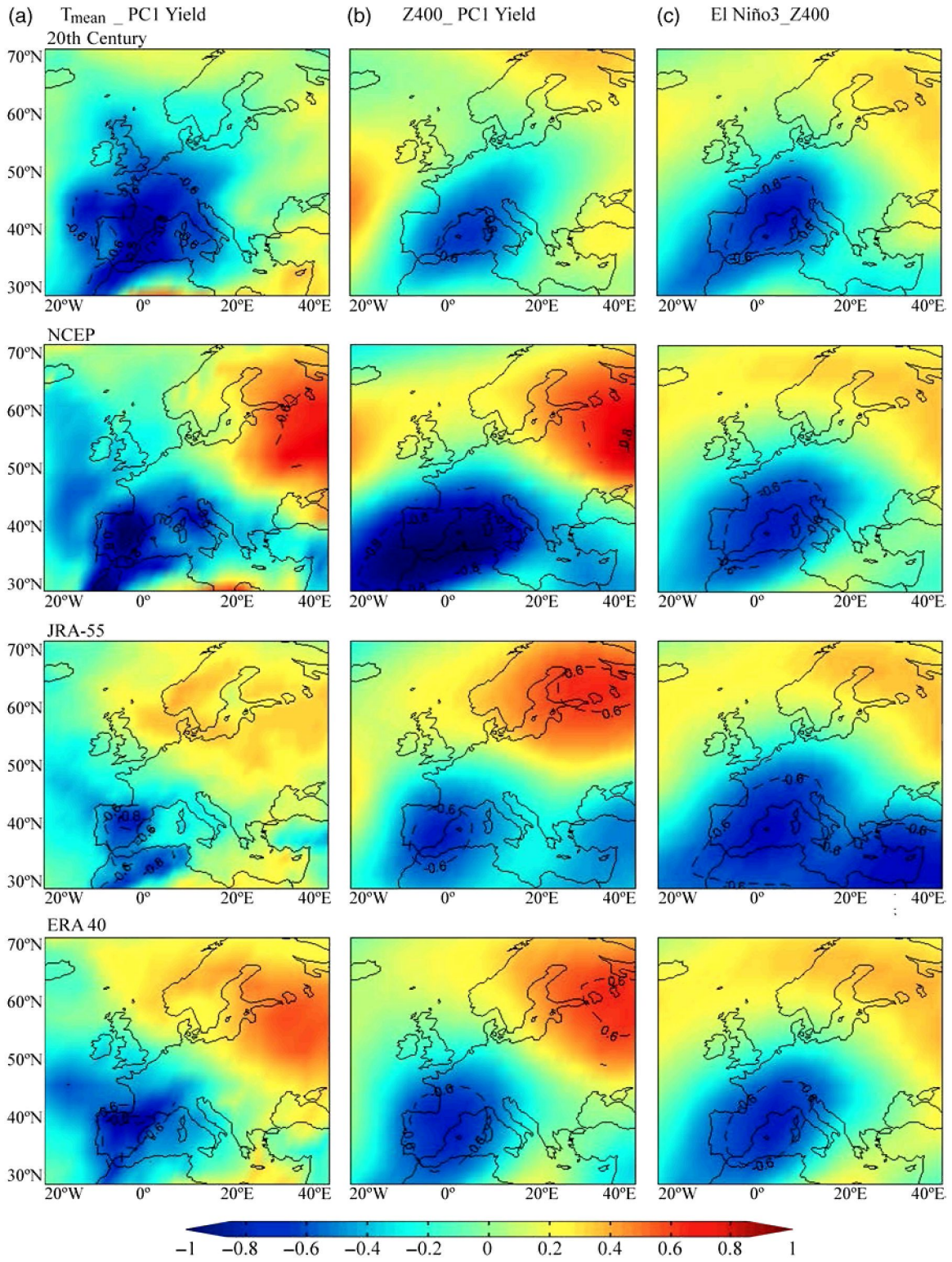

Figure 9. Spatial distribution of regression for 1960–1980 between (a) PC1 of maize yield anomalies in IP and JAS T_{mean} in Europe. Contours: ci = 0.2 °C per SD in the PC1. (b) PC1 of maize yield anomalies in IP and Z400 for JAS. Contours: ci = 0.2 hPa per SD in the PC1 (c) El Niño3 and Z400 for JAS. Contours: ci = 0.2 hPa per SD in the El Niño3 index. Statistical significant areas, according to a Monte Carlo correlation test at 95% confidence level, are in contour.

triggering teleconnections and consequently affecting the atmospheric variability in IP. T_{max} and T_{min} are the climate variables that have significant influence on irrigated maize yield in IP. The correlation with precipitation is not significant probably because the crop is provided with adequate water supply throughout the crop cycle. Therefore, precipitation does not influence yield in these simulations. The crop model only uses precipitation to calculate the amount of irrigation water required by crop. Several authors (Muchow *et al.*, 1990; Andrade *et al.*,

1993; Porter, 2005; Echarte *et al.*, 2013) have shown that temperature is the main determinant of the rate at which a plant progresses through the phenological stages towards maturity, affecting the cycle duration and thereby crop yield. The critical period, providing that flowering has taken place successfully, is the grain filling that occurs in IP around JAS. Negative anomalies of mean daily temperatures in this season are related to longer duration of grain filling, which means more assimilates (carbohydrates) allocated to the grain. This is a well-known eco-physiological mechanism: given all the other variables constant, longer grain filling implies higher crop yield as the crop has more time for doing photosynthesis and accumulating biomass in the harvestable fraction (Badu-Apraku *et al.*, 1983). Consequently, positive anomalies of grain filling duration are statistically related with positive anomalies of yield.

In addition, and still for 1960–1980, our results show that the Scandinavian pattern influences positively the yield and negatively the JAS T_{mean} of IP. This is in agreement with the Climate Prediction Center of NOAA (CPC: Climate Prediction Center, 2012), which shows that the positive phase of the Scandinavian pattern in summer is associated with above-average temperatures across Scandinavia and with below-average temperatures across IP and Mediterranean area. The Scandinavian pattern has a vigorous centre over Scandinavian Peninsula and an oppositely signed centre over Spain and the adjacent Mediterranean and Atlantic (Barnston and Livezey, 1987). Moreover, this result agrees with Toreti *et al.* (2010), who have found a significant negative correlation between the Scandinavian pattern and the summer temperatures in Italy, also in the Mediterranean area as IP. Therefore, El Niño is associated with a positive phase of the Scandinavian pattern, which produces positive yield anomalies in IP. Conversely, yield anomalies in IP are negative when the Scandinavian pattern is in negative phase, which happens in years of La Niña events.

Our results have important implications for crop forecasting, as we show that there is potential for characterizing the next crop season one year in advance depending on the events of El Niño phenomenon during the period when the forecast is performed. It is evident that an improvement of crop forecasting would benefit both public (agricultural planning) and private (decision support to farmers, insurance companies) sectors, helping to take advantage of favourable conditions or reducing the effect of adverse weather. Also, reducing the risk associated with increased climate variability is required for increasing productivity and quality while protecting the environment (Ogallo *et al.*, 2000).

5. Conclusions

Crop models are sensitive tools to detect climate variability and can reflect its effects on critical phases in crop development, whenever that reliable site-specific crop model calibration and validation with field data is accomplished. This study shows the utility of reanalysis data for obtaining long potential crop yield, only climate dependent, for the IP, as well as the need to be cautious in the use of reanalysis data in periods of early 20th century. Crop simulations performed with reanalysis data confirm the El Niño–yield relationships detected using the shorter observed climate datasets at all locations.

Our results highlight that a good percentage of maize yield variability can be explained with oceanic and atmospheric patterns. Most of the variability of irrigated maize yield in Spain can be explained by a homogeneous pattern with the same behaviour through the peninsula. Crop simulations show that there is a significant correlation between maize yield and El Niño Index. Nevertheless, the effects of El Niño on maize yield and T_{mean} in IP are non-stationary. El Niño event has a different impact on yields depending on the period and upon the phase change of El Niño that may occur between the spring and summer seasons.

The highest correlation between El Niño and yield took place in the period 1960–1980 (minimum of the AMO). For these decades, low yields were associated with an El Niño-to-La Niña transitions and high yields were associated with a La Niña to El Niño transitions. For these events, the regional associated atmospheric pattern resembles the Scandinavian one, which influences directly on the maximum and minimum temperatures experienced by the crop. This atmospheric pattern is part of the ENSO teleconnection pattern associated with El Niño.

The potential usefulness of this study is to apply the relationships found to crop forecasting on the next cropping season, suggesting opportunity time windows for the prediction. The methodology can be used as well for the prediction of future trends of IP yield variability. Both public and private sectors may benefit from such an improvement of crop forecasting.

Acknowledgements

The research by M. Capa-Morocho has been partly supported by a PICATA pre-doctoral fellowship from the Moncloa Campus of International Excellence (UCM-UPM) and the MULCLIVAR project (CGL2012-38923-C02-01 and CGL2012-38923-C02-02).

References

Andrade FH, Uhart SA, Cirilo A. 1993. Temperature affects radiation use efficiency in maize. *Field Crop. Res.* **32**: 17–25.

Badu-Apraku B, Hunter RB, Tollenaar M. 1983. Effect of temperature during grain filling on whole plant and grain yield in maize (*Zea mays L.*). *Can. J. Plant Sci.* **63**: 357–363.

Barnston AG, Livezey RE. 1987. Classification, seasonality and persistence of low-frequency atmospheric circulation patterns. *Mon. Weather Rev.* **115**: 1083–1126.

Brönnimann S. 2007. Impact of El Niño-Southern Oscillation on European climate. *Rev. Geophys.* **45**: RG3003.

Bueh C, Nakamura H. 2007. Scandinavian pattern and its climatic impact. *Q. J. R. Meteorol. Soc.* **133**: 2117–2131.

Bulic IH, Kucharski F. 2012. Delayed ENSO impact on spring precipitation over North/Atlantic European region. *Clim. Dyn.* **38**: 2593–2612.

Butterworth S. 1930. On the theory of filter amplifiers. *Exp. Wireless Wireless Eng.* **7**: 536–541.

Cadson RE, Todey DP, Taylor SE. 1996. Midwestern corn yield and weather in relation to extremes of the southern oscillation. *J. Prod. Agric.* **9**: 347–352, doi: 10.2134/jpa1996.0347.

Capa-Morocho M, Rodríguez-Fonseca B, Ruiz-Ramos M. 2014. Crop yield as a bioclimatic index of El Niño impact in Europe: crop forecast implications. *Agric. For. Meteorol.* **198–199**: 42–52.

Compo GP, Whitaker JS, Sardeshmukh PD, Matsui N, Allan RJ, Yin X, Gleason BE, Vose RS, Rutledge G, Bessemoulin P, Brönnimann S, Brunet M, Crouthamel RI, Grant AN, Groisman PY, Jones PD, Kruk MC, Kruger AC, Marshall GJ, Maugeri M, Mok HY, Nordli Ø, Ross TF, Trigo RM, Wang XL, Woodruff SD, Worley SJ. 2011. The twentieth century reanalysis project. *Q. J. R. Meteorol. Soc.* **137**: 1–28.

CPC: Climate Prediction Center. 2012. *Northern hemisphere teleconnection patterns*. http://www.cpc.ncep.noaa.gov/data/teledoc/telecontents.shtml (accessed 15 November 2014).

Dee DP, Uppala SM, Simmons AJ, Berrisford P, Poli P, Kobayashi S, Andrae U, Balmaseda MA, Balsamo G, Bauer P, Bechtold P, Beljaars ACM, van de Berg L, Bidlot J, Bormann N, Delsol C, Dragani R, Fuentes M, Geer AJ, Haimberger L, Healy SB, Hersbach H, Hólm EV, Isaksen L, Kållberg P, Köhler M, Matricardi M, McNally AP, Monge-Sanz BM, Morcrette JJ, Park BK, Peubey C, de Rosnay P, Tavolato C, Thépaut JN, Vitart F. 2011. The ERA-Interim reanalysis: configuration and performance of the data assimilation system. *Q. J. R. Meteorol. Soc.* **137**: 553–597.

Diaz HF, Hoerling MP, Eischeid JK. 2001. ENSO variability, teleconnections and climate change. *Int. J. Climatol.* **21**: 1845–1862.

Ebita A, Kobayashi S, Ota Y, Moriya M, Kumabe R, Onogi K, Harada Y, Yasui S, Miyaoka K, Takahashi K, Kamahori H, Kobayashi C, Endo H, Soma M, Oikawa Y, Ishimizu T. 2011. The Japanese 55-year reanalysis "JRA-55": an interim report. *SOLA* **7**: 149–152, doi: 10.2151/sola.2011-038.

Echarte L, Nagore L, Di Matteo J, Cambareri M, Robles M, Della Maggiora A. 2013. Grain yield determination and resource use efficiency in maize hybrids released in different decades. In Agricultural Chemistry, Stoytcheva M (ed). InTech, Rijeka, Croatia, 19–36.

Evans LT, Fischer RA. 1999. Yield potential: its definition, measurement, and significance. *Crop Sci.* **39**: 1544–1551, doi: 10.2135/cropsci1999.3961544x.

Gabaldon-Leal C, Lorite IJ, Minguez MI, Lizaso JI, Dosio A, Sanchéz E, Ruiz-Ramos M. 2015. Climate-change and extreme-temperature adaptation strategies for maize in Andalusia, Spain. *Climate Res.*, in press, doi: 10.3354/cr01311.

Gabriel JL, Quemada M. 2011. Replacing bare fallow with cover crops in a maize cropping system: yield, N uptake and fertiliser fate. *Eur. J. Agron.* **34**: 133–143.

Gimeno L, Ribera P, Iglesias R, de la Torre L, García R, Hernández E. 2002. Identification of empirical relationships between indices of ENSO and NAO and agricultural yields in Spain. *Clim. Res.* **21**: 165–172.

Godfray HCJ, Beddington JR, Crute IR, Haddad L, Lawrence D, Muir JF, Pretty J, Robinson S, Thomas SM, Toulmin C. 2010. Food security: the challenge of feeding 9 billion people. *Science* **327**: 812–818.

Greatbatch RJ, Lu J, Peterson KA. 2004. Nonstationary impact of ENSO on Euro-Atlantic winter climate. *Geophys. Res. Lett.* **31**: L02208.

Hammer G, Carberry P, Stone R. 2000. In *Applications of Seasonal Climate Forecasting in Agricultural and Natural Ecosystems*. Comparing the Value of Seasonal Climate Forecasting Systems in Managing Cropping Systems, Hammer GL, Nicholls N, Mitchell C (eds). Springer: Dordrecht, Netherlands, 183–195.

Handler A. 1990. USA corn yields, the El Niño and agricultural drought: 1867–1988. *Int. J. Climatol.* **10**: 819–828.

Hannachi A. 2004. A Primer for EOF Analysis of Climate Data. Department of Meteorology, University of Reading: Reading, UK, 33 pp.

Hoogenboom G, Jones JW, Wilkens PW, Porter CH, Boote KJ, Hunt LA, Singh U, Lizaso JL, White JW, Uryasev O, Royce FS, Ogoshi R, Gijsman AJ, Tsuji GY. 2010. *The Decision Support System for Agrotechnology Transfer (DSSAT). Version 4.5 [CD-ROM].* University of Hawaii: Honolulu, 51 pp.

Jones C, Kiniry J. 1986. *CERES-Maize: A Simulation Model of Maize Growth and Development*. Texas A&M University Press: College Station, TX, 194 pp.

Kalnay E, Kanamitsu M, Kistler R, Collins W, Deaven D, Gandin L, Iredell M, Saha S, White G, Woollen J, Zhu Y, Leetmaa A, Reynolds R, Chelliah M, Ebisuzaki W, Higgins W, Janowiak J, Mo KC, Ropelewski C, Wang J, Jenne R, Joseph D. 1996. The NCEP/NCAR 40-year reanalysis project. *Bull. Am. Meteorol. Soc.* **77**: 437–471.

Knippertz P, Ulbrich U, Marques F, Corte-Real J. 2003. Decadal changes in the link between El Niño and springtime North Atlantic oscillation and European–North African rainfall. *Int. J. Climatol.* **23**: 1293–1311.

Kottek M, Grieser J, Beck C, Rudolf B, Rubel F. 2006. World map of the Köppen-Geiger climate classification updated. *Meteorol. Z.* **15**: 259–263, doi: 10.1127/0941-2948/2006/0130.

Lizaso JI, Maturano M, Cela S, Lloveras J, Madrona FV. 2010. Evaluating CERES and IXIM, the maize simulation models in DSSAT v4.5 under irrigated Mediterranean conditions. In *XI th European Society for Agronomy Congress, AGRO 2010*, European Society for Agronomy, Montpellier, France, August 29 to September 03, 2010, S322–S236.

Lobell DB, Cassman KG, Field CB. 2009. Crop yield gaps: their importance, magnitudes, and causes. *Annu. Rev. Environ. Resour.* **34**: 179–204.

López-Cedrón FX, Boote KJ, Ruíz-Nogueira B, Sau F. 2005. Testing CERES-Maize versions to estimate maize production in a cool environment. *Eur. J. Agron.* **23**: 89–102.

López-Parages J, Rodríguez-Fonseca B. 2012. Multidecadal modulation of El Niño influence on the Euro-Mediterranean rainfall. *Geophys. Res. Lett.* **39**: L02704.

López-Parages J, Rodríguez-Fonseca B, Terray L. 2014. A mechanism for the multidecadal modulation of ENSO teleconnection with Europe. *Clim. Dyn.* **1**: 1–14, doi: 10.1007/s00382-014-2319-x.

Lorenzo MN, Taboada JJ, Iglesias I, Gómez-Gesteira M. 2011. Predictability of the spring rainfall in Northwestern Iberian Peninsula from sea surfaces temperature of ENSO areas. *Clim. Change* **107**: 329–341.

Mariotti A, Zeng N, Lau KM. 2002. Euro-Mediterranean rainfall and ENSO – a seasonally varying relationship. *Geophys. Res. Lett.* **29**: 59–61.

Maturano M. 2002. *Estudio del uso del agua y del nitrogeno dentro del marco de una agricultura sostenible en las regiones maiceras Castellano-Manchegas y Argentina*. PhD thesis, Department of Producción Vegetal y Tecnología Agraria, Castilla la Mancha University, Real, Spain, 292 pp.

Meinke H, Hammer G. 1995. Climatic risk to peanut production: a simulation study for Northern Australia. *Aust. J. Exp. Agric.* **35**: 777–780.

Muchow RC, Sinclair TR, Bennett JM. 1990. Temperature and solar radiation effects on potential maize yield across locations. *Agron. J.* **82**: 338–343.

Ogallo LA, Boulahya MS, Keane T. 2000. Applications of seasonal to interannual climate prediction in agricultural planning and operations. *Agric. For. Meteorol.* **103**: 159–166.

Phillips JG, Cane MA, Rosenzweig C. 1998. ENSO, seasonal rainfall patterns and simulated maize yield variability in Zimbabwe. *Agric. For. Meteorol.* **90**: 39–50.

Porter JR. 2005. Rising temperatures are likely to reduce crop yields. *Nature* **436**: 174–174.

Potgieter AB, Hammer GL, Doherty A, de Voil P. 2005. A simple regional-scale model for forecasting sorghum yield across North-Eastern Australia. *Agric. For. Meteorol.* **132**: 143–153.

Rodó X, Baert E, Comín FA. 1997. Variations in seasonal rainfall in Southern Europe during the present century: relationships with the North Atlantic Oscillation and the El Niño-Southern Oscillation. *Clim. Dyn.* **13**: 275–284.

Roe GH, Steig EJ. 2004. Characterization of millennial-scale climate variability. *J. Clim.* **17**: 1929–1944.

Rosenzweig C, Liverman D. 1992. Predicted effects of climate change on agriculture: a comparison of temperate and tropical regions. In *Global Climate Change: Implications, Challenges and Mitigation Measures*. Pennsylvania Academy of Sciences: Philadelphia, PA, 342–361.

Rozas V, Garcia-Gonzalez I. 2012. Non-stationary influence of El Niño-Southern Oscillation and winter temperature on oak latewood growth in NW Iberian Peninsula. *Int. J. Biometeorol.* **56**: 787–800.

Salinger MJ, Sivakumar MVK, Motha R. 2005. Reducing vulnerability of agriculture and forestry to climate variability and change: workshop summary and recommendations. *Clim. Change* **70**: 341–362.

Saue T, Kadaja J. 2009. Simulated crop yield – an indicator of climate variability. *Boreal Environ. Res.* **14**: 132–142.

Shin DW, Baigorria GA, Lim YK, Cocke S, LaRow TE, O'Brien JJ, Jones JW. 2010. Assessing maize and peanut yield simulations with various seasonal climate data in the Southeastern United States. *J. Appl. Meteorol. Climatol.* **49**: 592–603.

Smith TM, Reynolds RW, Peterson TC, Lawrimore J. 2008. Improvements to NOAA's historical merged land–ocean surface temperature analysis (1880–2006). *J. Clim.* **21**: 2283–2296.

Toreti A, Desiato F, Fioravanti G, Perconti W. 2010. Seasonal temperatures over Italy and their relationship with low-frequency atmospheric circulation patterns. *Clim. Change* **99**: 211–227.

Uppala SM, Kållberg PW, Simmons AJ, Andrae U, Bechtold VDC, Fiorino M, Gibson JK, Haseler J, Hernandez A, Kelly GA, Li X, Onogi K, Saarinen S, Sokka N, Allan RP, Andersson E, Arpe K, Balmaseda MA, Beljaars ACM, Berg LVD, Bidlot J, Bormann N, Caires S, Chevallier F, Dethof A, Dragosavac M, Fisher M, Fuentes M, Hagemann S, Hólm E, Hoskins BJ, Isaksen L, Janssen PAEM, Jenne R, McNally AP, Mahfouf JF, Morcrette JJ, Rayner NA, Saunders RW, Simon P, Sterl A, Trenberth KE, Untch A, Vasiljevic D, Viterbo P, Woollen J. 2005. The ERA-40 re-analysis. *Q. J. R. Meteorol. Soc.* **131**: 2961–3012.

Van Oldenborgh GJ, Burgers G, Tank AK. 2000. On the El Niño teleconnection to spring precipitation in Europe. *Int. J. Climatol.* **20**: 565–574.

von Storch H, Zwiers FW. 2001. *Statistical Analysis in Climate Research.* Cambridge University Press, Cambridge, United Kingdom, 484 pp.

Zanchettin D, Franks SW, Traverso P, Tomasino M. 2008. On ENSO impacts on European wintertime rainfalls and their modulation by the NAO and the Pacific multi-decadal variability described through the PDO index. *Int. J. Climatol.* **28**: 995–1006.